THE JOURNAL OF PHYSICAL CHEMISTRY C

Article

pubs.acs.org/JPCC

Influence of Crystal Structure of Bulk Phase on the Stability of Nanoscale Phases: Investigation on MgH_2 Derived Nanostructures

P. Vajeeston,*[,†,‡] P. Ravindran,[†,§] M. Fichtner,[∥] and H. Fjellvåg[†]

[†]Center for Materials Science and Nanotechnology, [‡]Center of Theoretical and Computational Chemistry, Department of Chemistry, University of Oslo, Box 1033 Blindern, N-0315, Oslo, Norway

[§]Department of Physics, Central University of Tamil Nadu, Thiruvarur 610 004, Tamil Nadu, India

[∥]Institute for Nanotechnology, Karlsruhe Institute of Technology, D-76021 Karlsruhe, Germany

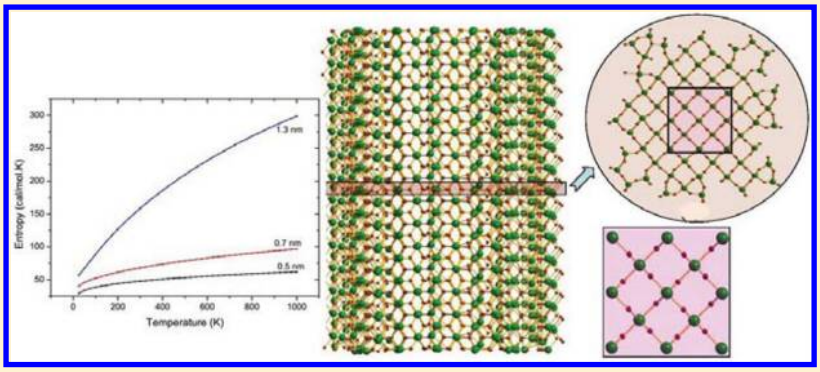

ABSTRACT: Phase stability of α-, β-, γ-, and δ'-MgH_2-derived nanostructures have been investigated using ab initio projected augmented plane wave method. Structural optimizations based on total energy calculations predicted that β-derived nanoparticles and α-derived nanowhiskers are more stable than those derived from other polymorphs. Present study indicates that the crystal structure of the bulk phase plays a significant role on the stabilization of different forms (nanoparticles or nanowhiskers) of nanophases. The predicted critical sizes of the stable β-nanoparticle and α-nanowhisker for MgH_2 are 2.4 and 1.5 nm, respectively. The calculated hydrogen site energies suggest that it is relatively easier to remove hydrogen from the surface of the nanoparticles and nanowhiskers compared to that from bulk crystals. Among the considered nano-objects, removing hydrogen from the β-derived nanocluster is much easier, and hence, the present study suggests that one can use these nanoparticles for practical applications. NMR-related parameters are calculated for different sizes of the nanoclusters and nanowhiskers.

I. INTRODUCTION

In general, nano structure is classified as a material structure assembled from a layer or cluster of atoms with a size in the order of nanometers. Interest in various fields at size scales larger than that of atoms and smaller than that of bulk solids (mesoscopic physics) has grown rapidly since the 1970s, owing to the increasing realization that the properties of these mesoscopic atomic ensembles are different from those of conventional solids. As a consequence, interest in artificially assembling materials from nanometer-sized building blocks has risen. Because many studies have shown that, by controlling sizes (in the range of 1−100 nm) and assembly of constituents, it was possible to alter and prescribe properties of such assembled nano structures. These nanostructured materials are modulated over nanometer length scales in zero to three dimensions. They can be assembled with modulation dimensionalities of zero (e.g., atomic clusters),[1,2] one (e.g., chains),[3] two (e.g., ultrafine-grained overlayers or coatings or buried layers),[2] and three (nanophase materials)[2,4] or with intermediate dimensionalities.

In the bulk state a solid material may exist in more than one form or crystal structure (called polymorphs). These polymorphs may have different stabilities and may spontaneously convert from a metastable form (unstable form) to the stable form at a particular temperature and pressure. They may also exhibit different melting points, solubilities, physical properties, X-ray diffraction patterns, and so on. For example, AlH_3 is a unique binary hydride that has at least six crystalline phases (depending on the synthesis route) with different physical properties and at the same time store up to 10.1 wt % of hydrogen.[5] MgH_2 is also an attractive material for hydrogen-storage applications because of its lightweight, low manufacture cost, and high hydrogen-storage capacity (7.66 wt %), which has at least two polymorphs at ambient conditions. However, its slow hydriding/dehydriding kinetics and high dissociation temperature (nearly 573 K) prevent its practical applications on auto mobile technologies. In our recent experimental study[6] we have found that application of pressure on α-MgH_2 transforms it into γ-to-β and β-to-δ' modifications. Numerous studies have been focused on MgH_2 for improving the problematic sorption

Received: December 6, 2011
Revised: August 21, 2012
Published: August 21, 2012

   dx.doi.org/10.1021/jp305933g | J. Phys. Chem. C 2012, 116, 18965−18972

kinetics, including mechanical ball milling,[7−12] doping,[10,13−16] and chemical alloying.[15,17−21] Though, it is found that these methods considerably improve absorption and desorption kinetics, they are not sufficient for practical onboard applications. In this present work we have carried out stability study on nanophases of α-, β-, γ-, and δ'-MgH_2 modifications. We also addressed the issues such as structure of the nanophase objects and the role of crystal structure of bulk phase on nanophase formation.

II. COMPUTATIONAL DETAILS

Total energies have been calculated by the projected-augmented plane-wave (PAW)[22] implementation of the Vienna ab initio simulation package (VASP).[23] All these calculations are made with the generalized gradient approximation of the Perdew, Burke, and Ernzerhof (PBE)[24] exchange correlation functional. It should be noted that both PW91[25] and PBE functionals gave almost the same result. The differences in the energetics and structures of using these two functionals were found to be negligible, and hence, the results reported here were computed with the PBE functional. Ground-state geometries were determined by minimizing stresses and Hellman-Feynman forces using the conjugate-gradient algorithm with force convergence less than 10^{-3} eV Å^{-1}. Brillouin zone integration was performed with a Gaussian broadening of 0.1 eV during all relaxations. From various sets of calculations it was found that 500 k points in the whole Brillouin zone for the α-MgH_2 structure with a 500 eV plane-wave cutoff are sufficient to ensure optimum accuracy in the computed results. A similar density of k points and energy cutoff were used for β, γ, and δ' modifications.

Different sizes of the nanoparticles and nanowhiskers have been constructed from optimized bulk phases using supercells of varying sizes. The k-points were generated using the Monkhorst-Pack method with a grid size of 1 × 1 × 1 and 2 × 2 × 1, for structural optimization for nanoparticle and nanowhiskers, respectively. During the nanoparticle/whisker construction the MgH_2 stoichiometry was always maintained. For the nanowhisker construction, the vacuum is included only in the x and y directions. On the other hand, for the nano cluster construction, the vacuum is included in the x, y, and z directions. The vacuum thickness was considered wide enough to prevent whisker-to-whisker or cluster-to-cluster interactions and we found that a width of 12 Å was sufficient to ensure that the energy was converged to less than 1 meV/atom.

The NMR parameters are computed using the CASTEP code.[26] For the CASTEP computation we have used the optimized structures obtained from VASP as input. Norm-conserving pseudopotentials and the generalized gradient approximation (GGA) exchange correlation functional proposed by PBE were used.[27]

III. STRUCTURAL ASPECTS

α-MgH_2 crystallizes in the rutile-type structure ($P42/mnm$) at ambient conditions.[28,29] At higher temperatures and pressures, α-MgH_2 transforms into the orthorhombic γ-MgH_2 modification (α-PbO_2; $Pbcn$). It should also be noted that Bortz et al. investigated the crystal structure of γ-MgH_2 from powder neutron-diffraction data collected at 2 GPa.[30] This high-pressure γ modification is maintained as the metastable phase when the pressure is released at room temperature after a completed pressure loading−unloading cycle. Many density functional theory (DFT) studies have attempted to predict the effect of pressure on the phase transitions for the polymorphs of MgH_2, but no general agreement on the results was obtained. Vajeeston et al.[31] have investigated pressure-induced structural transitions in MgH_2[31] using the first-principles pseudopotential method and predicted that the transition from α-MgH_2 to γ-MgH_2 occurs at 0.39 GPa. On the other hand, Cui et al.[32] obtained 1.2 GPa for the same transition. Under further compression, several other high-pressure phases (with space group $Pa\bar{3}$, $Pbc21$, $Pbca$; $Pnnm$, $Fm3\bar{m}$) were proposed by theory,[6,33] and the ab initio pseudopotential calculations established the sequence of the phase transition as $\alpha \rightarrow \gamma \rightarrow \beta(Pa\text{-}3) \rightarrow \delta(Pbc21) \rightarrow \varepsilon(Pnma)$.[6,31] Recently, a metastable phase of MgH_2 ($I41/amd$, space group 141), which meets all the mechanical stability criteria for a tetragonal crystal, has been suggested through full-potential linearized augmented plane-wave (FP-LAPW) calculations.[34] Very recently, a new pressure-induced transition from the α-MgH_2 phase to an orthorhombic $CaCl_2$ ($Pnnm$) phase is predicted by ab initio phonon calculations.[35] Experimentally also no apparent agreement has been reached on the pressure values for these phase changes. Bastide et al.[28] reported coexistence of α- and γ-MgH_2 in the 2−8 GPa range with no common pattern for the formation of β-MgH_2. Bortz et al.[30] studied the crystal structure of γ-MgH_2 (ex situ) synthesizing this phase at high temperature (1000 K) and at 2 GPa pressure but without achieving full transformation of α into γ; Vajeeston et al.[6] reported the full α−γ phase transition as occurring at 5.5 GPa at room temperature (RT),a γ−β transition at 9 GPa and β to δ' at above 10 GPa; upon decompression, β and γ coexisted without transforming back to α: Kohlmann et al.[36] did not report any transformation into the γ phase up to 9.3 GPa, and finally, Moser et al.[37] reported the formation of γ-MgH_2 at 4.3 GPa and 450 K but with no transformation back into α-MgH_2. To solve these issues and to further understand the high pressure behaviors of MgH_2, more careful experimental and theoretical efforts are needed.

The primitive cell of α-MgH_2 contains two Mg and four H atoms. Each Mg atom is octahedrally coordinated to six H atoms, whereas each H atom is coordinated to three Mg atoms in the same plane. In β-, γ-, and δ'-MgH_2 polymorphs, Mg atom is octahedrally coordinated by six H atoms. Both in the γ and δ' polymorphs, these octahedra are strongly distorted and the Mg−H bond lengths and H−Mg−H bond angles are very different. The energy difference between the α and γ modifications is very small at the equilibrium volume indicating the possibility of stabilizing both the phases. Structurally also α- and γ-MgH_2 are closely related (for more detail, see refs 6 and 30). It may be noted that the calculated results are valid only for defect-free ideal single crystal at low temperatures.

IV. STUDIES ON NANOPARTICLES

The optimized stable α-, β-, γ-, and δ'-MgH_2 derived nanoparticles are displayed in Figure 1. From the variation in the interatomic distances of the nanoparticles compared with that of the bulk phases, it should be anticipated that nanophase materials have different physical and chemical properties from the bulk materials. We calculated the total energies by reducing the particle size over a certain range. The particle size beyond which the total energy remains constant is defined as the "critical particle size" where most of the atoms will be exposed to the surface. According to the pair distribution function, we found that in most of these cases ∼90% atoms are in the

dx.doi.org/10.1021/jp305933g | J. Phys. Chem. C 2012, 116, 18965−18972

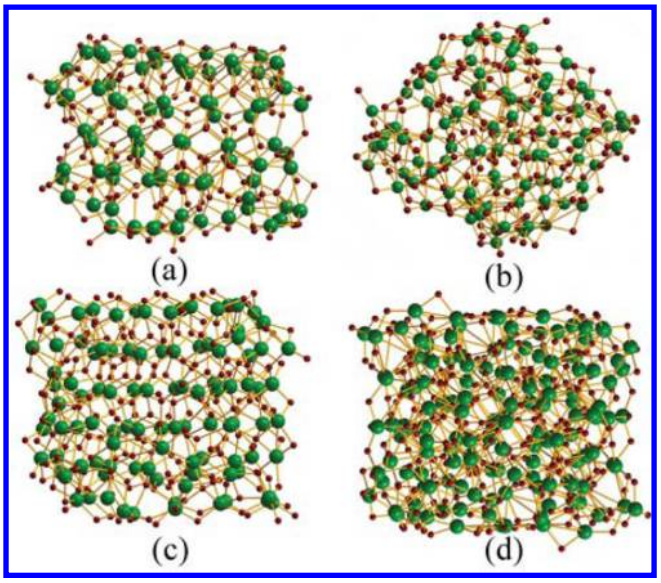

Figure 1. Optimized stable nanocluster of MgH_2, derived from (a) α-, (b) β-, (c) γ-, and (d) δ'-MgH_2 phases. The Mg atoms are presented in dark green and H atoms are represented in dark red color.

surfaces. To identify the critical particle size and relative stability of the nanoparticle, we have calculated the total energy as a function of the cluster size for the different polymorph-derived particles, and the results are shown in Figure 2. It is

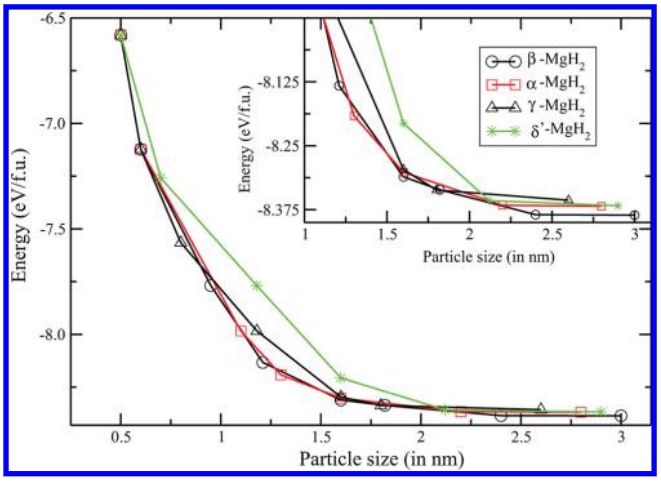

Figure 2. Calculated total energy (in eV/f.u.) as a function of cluster size for α- (red quare), β-(black circle), γ- (black triangle), and δ'-(green star) MgH_2 derived nanoparticles. Magnified version is shown in the inset figure.

evident that β-derived nanoparticles with a cluster size above 2.4 nm are lower in energy than the other polymorph-derived particles. However, the involved energy difference between the different types of particles is very small (in the range of 1.7−2.9 kJ/mol; see Table 1). This closeness in energy suggests that the relative appearance of these modifications will be quite sensitive to, and easily affected by, other external factors such as temperature, pressure, and so on. In the present calculation the temperature effect was not taken into account. Because of the large number of atoms involved in the calculation, it is not possible to do the dynamical stability for such a big system. However, from our experience in this field we found that if the calculated particle size varies as a function of the total energy

Table 1. Calculated Critical Nanowhisker Diameter, Nanoparticle Size (in nm), and Relative Energy (in kJ/mol f.u.) for the Bulk (Calculated at the Equilibrium Volume), Stable Nanowhisker and Nanoparticles of MgH_2 Polymorphs

	bulk phase	nanoparticle		nanowhisker	
modification	relative energy	critical size	relative energy	critical diameter	relative energy
α-derived	0.0	2.2	1.7	1.5	0.0
β-derived	9.01	2.4	0.0	1.65	2.4
γ-derived	0.15	1.8	2.9	1.42	1.8
δ'-derived	7.37	2.1	1.8	1.83	11.92

very smoothly then one can qualitatively judge that the optimized particle is stable (at least closer to the equilibrium). In all our total energy calculation we have used the same computational parameters. Hence, the error in the calculation will be the same in all calculations that are smeared out when we compare the relative energies. To understand the changes in entropy with respect to the size of the nanostructures, we have calculated the entropy for a selected nanoparticle constructed from the α-MgH_2 with sizes 0.5, 0.7, and 1.3 nm. The calculated entropy as a function of temperature for the selected nanoparticles is shown in Figure 3 (left-hand side). To understand the relative change in the entropy, we have also displayed the entropy of the selected nanoparticles and bulk α-MgH_2 at 300 K (see Figure 3, right-hand side). Figure 3 clearly demonstrates that when the particle size becomes smaller the systems are destabilized. This finding is consistent with our total energy calculations. It can be noted that, if the particle size is considerably big, several stable modifications may be possible. It is important to note that, when we reduce the particle size below 1.5 nm, all the polymorph-derived nanoparticles are having almost similar energy, especially in the 0.5−1 nm range. It implies that, even though the nanoparticles are constructed from different bulk polymorphs, all are converged toward a similar type of particles, where all the atoms are almost in the surface without any core structural units representing the bulk phases in such objects.

When the nanoparticle size is between 1.5 and 2.25 nm range, the α, β, and γ-MgH_2 derived nanoparticles are very close in energy and the competition between these phases is almost indistinguishable. This suggests that the particle size variation may change the structure of the nanophase. It may be noted that, in zirconia nanoparticles, if the critical particle size exceeds 30 nm, the tetragonal phase is transformed to the monoclinic phase.[38] A common feature noticed in Figure 2 is that, if the cluster size decreases, the total energy becomes more positive in all the polymorph-derived particles (i.e., the formation energy decreases with decrease in the cluster size). In particular, there is a steep increase in the total energy when the size of the cluster is smaller than 1.75 nm. The calculated critical particle/cluster size of the different polymorphs varies from 1.8 to 2.4 nm (with minimum value for γ- and maximum for the β-derived nanoparticle). The predicted critical particle size for the α-MgH_2 is consistent with other theoretical works published in the literature.[39−41] This finding clearly demonstrates that, when nanoparticles of MgH_2 are prepared, it prefers to stabilize in β-phase with particle size more than 2.4 nm. For bulk phases it is generally believed that cubic modification may have lower decomposition and better kinetics than other modifications. The stabilization of β-polymorph derived nanoparticles receives special attention in this respect.

dx.doi.org/10.1021/jp305933g | J. Phys. Chem. C 2012, 116, 18965−18972

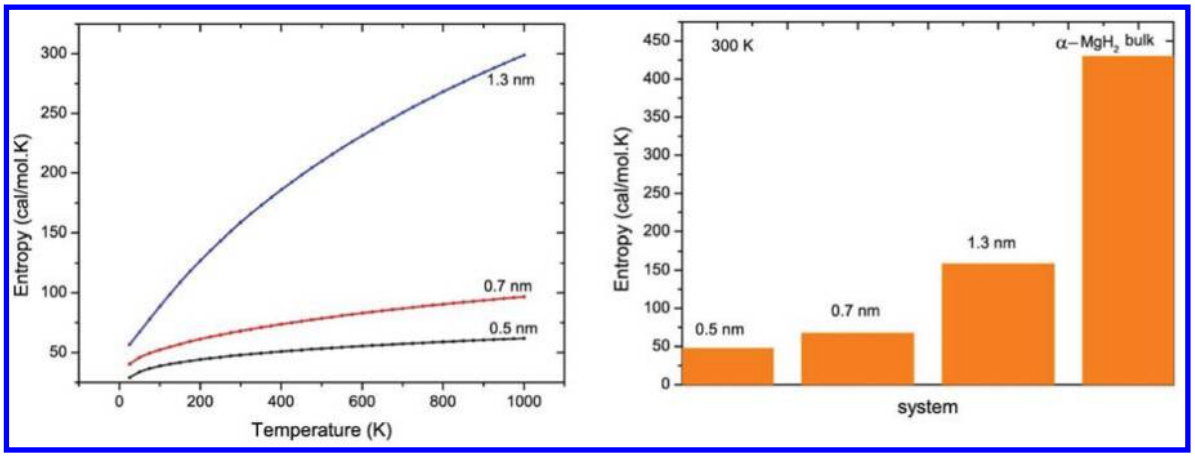

Figure 3. Calculated temperature vs entropy plot for α-MgH_2 derived nanoparticles (only selected size; left-hand side). Entropy changes at 300 K for the selected nanoclusters and bulk α-MgH_2 phase (right-hand side).

If this high-pressure phase is stabilized at ambient condition in nanophases or in some other form, it might have better hydrogen-storage properties than the other polymorphs like α- and γ-MgH_2. Recently, Kyoi et al. synthesized the Mg_7TiH_x phase at high pressure (8 GPa) and high temperature (873 K) and this phase crystallizes in cubic form ($Fm\bar{3}m$).[42] The hydrogen desorption temperature for this compound is about 130 K lower than that of bulk phase of MgH_2. It is interesting to note that the crystal structure of Mg_7TiH_x is a super structure of the high pressure β-modification. From this point of view the predicted stable nanoparticles based on β-phase might have better hydrogen storage properties than the bulk phase. Moreover, it is challenging to prepare bare nanoparticles of MgH_2 by existing experimental techniques. Even if bare nanoparticles are made, they could agglomerate and form large entities which do not exhibit a size effect anymore. Alternatively one can prepare/isolate such types of particles in porous scaffold structures. When MgH_2 is incorporated into carbon aerogel scaffolds with pore sizes of 13 nm, a significant increase in dehydrogenation rates was observed.[43,44] However, there was no significant change in the thermodynamic properties for MgH_2 confined within 13 nm pores.[43,44] Recently, Lu et al.[15] prepared nanostructured MgH_2–$0.1TiH_2$ material system by ultrahigh-energy-high-pressure mechanical milling. The grain size of the milled powder is approximately 5–10 nm with uniform distributions of TiH_2 among MgH_2 particles. The authors demonstrated that addition of TiH_2 significantly improved the kinetics of dehydrogenation and hydrogenation compared to MgH_2. More importantly, the MgH_2–$0.1TiH_2$ material system showed excellent cycle stability. Similarly, Cuevas et al. synthesized MgH_2–TiH_2 nanocomposites by ball milling of elemental powders under 8 MPa of hydrogen pressure.[45] The composites consist of a mixture of β-rutile MgH_2, γ-orthorhombic high pressure MgH_2, and ε-tetragonal TiH_2 phases with nanosized crystallites ranging from 4 to 12 nm.[45] This MgH_2–TiH_2 nanocomposite exhibits outstanding kinetic properties and cycling stability.[45] Nanocrystals of MgH_2 (~7 nm in size) embedded in a matrix of LiCl were reported by Paskevicius et al.[46] using mechanochemical metathesis reaction between $MgCl_2$ and LiH.[46] In this study the enthalpy (ΔH) was decreased by 2.84 kJ/mol H_2, from 74.06 ± 0.42 kJ/mol H_2 for the bulk to 71.22 ± 0.49 kJ/mol H_2 for the 7 nm crystals. The entropy (ΔS) also decreased from 133.4 ± 0.7 J/k mol H_2 to 129.6 ± 0.8 J/k mol H_2. These results agree with density functional theory (DFT) calculations on Wulff construction nanocrystals, which indicate that <10 nm particles sizes (<5 nm radii) are needed for any noticeable enthalpy change of the order of ~1 kJ/mol H_2.[41] Recently, Zhao-Karge et al. demonstrated that MgH_2 particles with a smaller particle size (<3 nm) exhibit significant changes in H and S, which were reduced by 11 and 19 kJ mol^{-1}, respectively.[47] These results reflect a size effect on reducing the thermodynamic stability of MgH_2 and consistent with our present study. In our present calculation we found that the critical particle size (where one can expect the dehydrogenation enthalpy decreased from the bulk value) size of the clusters and whiskers are smaller than 2.4 and 1.5 nm, respectively. However, these results pertain to free MgH_2 clusters/whiskers, whereas, experimentally, the nano-confined MgH_2 is bound to scaffolds that introduce the effects of interfacial energies. While further work is required to fully understand the effect of nanoconfinement on MgH_2, it appears that changes in thermodynamic stability will be small for confinement at ≥5 nm. Much smaller confinement (~1–2 nm) may be required for significant alteration.

The calculated Mg–H distances versus number of bonds (i.e., the pair distribution function, see Figure 4) for the

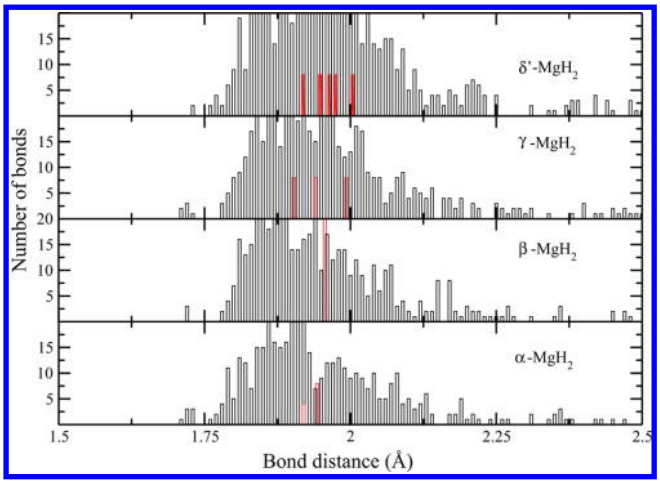

Figure 4. Calculated interatomic distances between Mg–H in the optimized nanoparticles of MgH_2 derived from α-, β-, γ-, and δ'-MgH_2 phases. The corresponding Mg–H distances in the bulk phases are noted in red color.

dx.doi.org/10.1021/jp305933g | J. Phys. Chem. C 2012, 116, 18965–18972

optimized nanoparticles indicate that the values are very scattered compared to that in the corresponding bulk phases. The corresponding Mg−H distances in the bulk phases are denoted in red color (see Figure 4). Especially, several Mg−H bonds in the nanoparticles have longer and shorter bond distances than that in the corresponding bulk phases. This type of structural arrangement is expected in nano and amorphous phases with no three-dimensional crystallinity.

V. STUDIES ON NANOWHISKERS

A systematic investigation on the total energy as a function of dimension of α-, β-, γ-, and δ'-MgH_2 derived nanowhiskers shows almost (not shown in figure) a similar behavior as that in nanoparticles except for the stability sequence. In contrast to the nanoparticles where the β-phase derived nanoparticles have the lowest energy, the α-MgH_2 derived nanowhiskers have lower energy than those derived from other polymorphs. This is in agreement with experimental studies by Zlotea et al.[48] and Saita et al.[49] By hydrogen absorption and subsequent disproportionation of bulk $Mg_{24}Y_5$, Zlotea et al.[48] found the formation of one-dimensional single crystalline MgH_2 phases with nanometer and micrometer ranges. These nanowires/whiskers have been structurally and morphologically characterized by X-ray diffraction[48] and scanning as well as transmission electron microcopies.[49] Saita et al.[49] also found the formation of such one-dimensional needle-shaped single crystalline MgH_2 using a chemical vapor synthesis technique. The formation energy of nanowhisker decreases with decrease of nanowhisker diameter. In particular, there is a steep increase in the total energy when the diameter of the whisker is below 1.5 nm. The relative energy changes compared to the α-derived nanowhisker are much higher than that in the nanoparticle case (see Table 1). The calculated critical whisker diameter of the different polymorphs vary from 1.42 to 1.83 nm (with minimum value for γ- and maximum for the δ'-derived nanowhiskers).

To understand the internal atomic arrangements of the stable nanowhiskers (Figure 5a) we have analyzed the cross view (Figure 5b) of the biggest nanowhisker. From Figure 5 it is evident that the H−Mg−H atomic arrangement in the inner part of the nanowhisker is almost similar to that in the bulk α-MgH_2 phase (see Figure 5b,c). A closer inspection of the Mg−H distance in the nanowhiskers reveals that the Mg−H distance at the center of the whisker is still maintained as that of bulk (1.93 Å). Interestingly, some of the Mg−H bond lengths are shorter than that in the bulk γ-MgH_2 phase (1.91 Å). On the other hand, in the surface of the whisker, the calculated Mg−H distances are much higher than that in the bulk phases. This indicates that the bonding interactions in surface layers are considerably weaker than that at the center of the whisker. As a result, one can expect that the removal of hydrogen from the surface of the whisker is much easier than that from the bulk or from the inner part of the whisker. To substantiate this observation we have calculated the H site energy (HSE; ΔE) for these nanophases. In the nanoparticle/whisker H is situated in three different chemical environments; viz., E1 (center of the cluster/whisker); E2 (H in Mg−H−Mg bridge site) and E3 (Mg−H top site). The H site energy is calculated in the following manner $\Delta E = (E_{Hvac} + 1/2E_{Hmol}) - (E_{nano})$, where E_{Hvac} and E_{nano} refer to the energy of the nano-object with and without H vacancy and E_{Hmol} is the total energy of a free H_2 molecule calculated in a large box. For the HSE study we have used optimized biggest cluster (2.8, 3.0, 2.6, and 2.9 nm for α-, β-, γ-, and δ'-MgH_2 derived particles, respectively) and whiskers (diameters 1.9, 2.1, 1.8, and 2.2 nm for α-, β-, γ-, and δ'-MgH_2 derived whiskers, respectively). The calculated HSE for the bulk phase varies from 0.86 to 1.30 eV (minimum for the α-phase and maximum for γ-phase; see Table 2). The calculated HSE for nanoparticle and nanowhiskers are scattered over a wide energy range (see Table 2), highly depending on the environment of the H sites. In general, the calculated HSE for the E1 site for different MgH_2 polymorph-derived particles and whiskers have almost a similar value to that of their corresponding bulk phases. This is quite natural because all these nano-objects are maintaining their bulk atomic arrangement in their core/inner part. This finding clearly indicates that the energy required to remove H from the center of the nanophase (cluster/whisker) is similar to that in the bulk

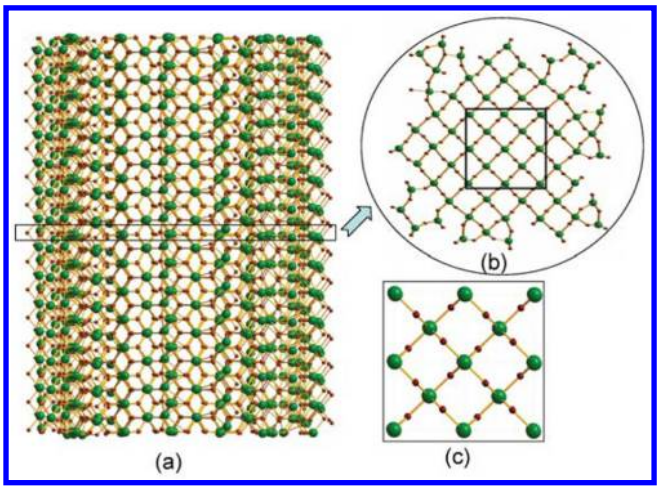

Figure 5. (a) Equilibrium structure of stable nanowhisker of MgH_2 derived from the bulk α-MgH_2 phase. (b) Internal H−Mg−H structural arrangement of MgH_2 in the optimized nanowhisker. (c) H−Mg−H structural arrangement in the bulk α-MgH_2 phase. The Mg atoms are presented in dark green and H atoms in dark red color.

Table 2. Calculated Hydrogen Site Energy (HSE; in eV) for the Bulk, Nanowhisker, and Nanoparticles of MgH_2 Polymorphs[a]

phase	bulk	nanoparticle	nanowhisker
α-MgH_2			
E1	0.86	0.848	0.858
E2		0.72	0.68
E3		0.78	0.78
β-MgH_2			
E1	1.078	0.98	1.06
E2		0.54	0.643
E3		0.68	0.97
γ-MgH_2			
E1	1.302	1.31	1.28
E2		0.83	0.794
E3		0.89	0.85
δ'-MgH_2			
E1	1.15	1.01	1.11
E2		0.75	0.68
E3		0.79	0.74

[a]E1 refers to H in center of the nanoparticles/whisker, E2 for H in the Mg−H−Mg bridge site, and E3 for H in Mg−H top site.

dx.doi.org/10.1021/jp305933g | J. Phys. Chem. C 2012, 116, 18965−18972

material. In all these studied systems, the HSE for H at E2 is always lower than that in E1 and E3. Moreover, the HSE values vary in the following sequence E2 < E3 < E1. The small values of hydrogen site energies in the surfaces of the nanophases compared with that in bulk material indicate that one can remove hydrogen relatively easily from the nanophases. However, when we remove H from the surface of the nanophase materials, the H atoms at the inner part may easily move/migrate to the surface (due to the size effect) and make the system to behave different from that of the bulk phase. It may be noted that this HSE result is obtained from the constrained calculation where temperature/vibrational effect is not included. The calculated HSE for the nanoparticles suggests that the energy required to remove hydrogen from the surface layers of β-MgH_2-derived nanoparticles is very small. In addition, the total energy calculations show that these nanoparticles are more stable than the nanoparticles derived from other phases. This finding clearly indicates that the nanostructures derived from β-MgH_2 will have more advantageous properties to use for practical applications because they substantially reduce the hydrogen sorption temperature and improve the kinetics.

VI. NMR STUDIES ON NANOPHASES

NMR is often used as an analytical tool to aid in structure prediction. Even though the general features of the crystal structure are understood, a detailed analysis of the geometry of nanophases proves elusive. When the calculated NMR parameters are used, it is possible to simulate the NMR spectrum for a series of related structures until a match is found between the computed and experimental results. In this way theory complements experiment by contributing to the determination of the correct crystal structure. If one could use both experiment and theory, NMR parameters can be used not only for structural analysis of bulk materials and nanophase materials, but also to characterize individual phases in a mixed-phase system. In this connection we have calculated the isotropic chemical shielding (σ_{iso}), quadrupolar coupling constant (C_Q), and quadrupolar asymmetry parameter (η_Q) for different polymorphs of MgH_2 and their nanophases using the following relations.

$$\sigma_{iso} = (\sigma_{xx} + \sigma_{yy} + \sigma_{zz})/3 \quad (1)$$

$$C_Q = eQV_{zz}/h \quad (2)$$

$$\eta_Q = (V_{xx} - V_{yy})/V_{zz} \quad (3)$$

where σ refers to the chemical shielding tensor in the principal axis frame. This is an absolute value of the isotropic chemical shielding, not relative to any standard. V_{zz} is the largest component of the diagonalized EFG tensor, Q is the nuclear quadrupole moment, and h is Plank's constant.

The calculated values of σ_{iso}, C_Q, and η_Q for the different polymorphs are displayed in Table 3. The calculated σ_{iso} values for Mg are scattered between 549 to 556 ppm. Similarly, for the hydrogen atoms in different polymorphs these values are scattered between 25.4 to 26.6 ppm and one cannot compare these values directly to the experimental values. Because the calculated values are absolute chemical shielding whereas the experimental value are concerned with shifts relative to a known standard. However, one can compare the comparative shifts between the different peaks. Similarly the C_Q and η_Q values are also scattered over a wide range and these values are directly comparable with experimental values. Unfortunately, no experimental values are yet available for comparison for the bulk phases, the present study will hopefully motivate experimental investigations of NMR spectra for different polymorphs of MgH_2. It should be noted that the NMR parameters are strongly related to the atomic environment (near neighbors) and quadrupolar coupling constants are directly related to the bond strength and anisotropy in the charge density distribution around the probe nuclei. In this connection, we have calculated NMR related parameters only for the stable α-derived nanowhiskers (for size 1.6 nm) and β-derived nanoparticles (of 2.4 nm size cluster). As calculation of the NMR parameters requires higher accuracy for the wave functions, we have performed very accurate computation to obtain reliable values. The calculated values of σ_{iso}, C_Q, and η_Q for the nano-objects are given in Table 3. As we have shown in the previous section, the bond length values are very scattered in the nanophases and also the NMR-related parameters are highly dependent on the local environment of the system. Hence, the calculated σ_{iso}, C_Q, and η_Q values for both nano-objects are highly scattered (see Table 3). For example, the calculated σ_{iso} value for Mg in the nanowhisker varies between 548 to 593 ppm and the corresponding value in nano particles varies between 542 to 581 ppm. Similarly the calculated σ_{iso} value for H in the nanowhisker varies between 22 to 26.9 ppm and the corresponding value in nano particles between 21.4 to 27.2 ppm. To understand the changes on NMR parameters as a function of particle size, we have calculated the NMR parameters for the selected nanowhiskers (α- derived; size: 0.6, 1, and 1.6 nm) and nanoparticles (β-derived; size: 0.6, 1.6, and 2.4 nm). Due to the close similarity in the chemical shielding of Mg and H in nanowhiskers and nanoparticles, we have displayed only the nanowhiskers chemical shielding corresponding to Mg and H in Figure 6. It is clear that depending on the particle size the calculated chemical shielding varies considerably and the values are well scattered. If the system becomes considerably bigger, the calculated chemical shielding is well broadened owing to the bulk-like core structure formation. On the other hand, in a smaller whisker/particle the chemical shielding becomes very narrow. The

Table 3. Computed Isotropic Chemical Shielding (σ_{iso}; in ppm), Quadrupolar Coupling Constant (C_Q; in MHz), and Quadrupolar Asymmetry (η_Q) for Different MgH_2 Polymorphs

parameter	element	σ_{iso} (ppm)	C_Q (MHz)	η_Q
α-MgH_2	Mg	549	2.06	0.31
	H	26.6	0.037	0.6
β-MgH_2	Mg	556	4.43	0
	H	25.4	0.034	0
γ-MgH_2	Mg	551	1.17	0.06
	H	26.4	0.035	0.73
δ'-MgH_2	Mg	552	3.06	0.81
	H1	25.7	0.032	0.37
	H2	26.1	0.35	0.69
α-MgH_2 derived whisker (1.6 nm)	Mg	548−593	1.16−8.67	0.22−0.58
	H	22−26.9	0.0095−0.038	0.25−0.98
β-MgH_2 derived cluster (2.4 nm)	Mg	542−581	1.86−7.21	0.0−0.34
	H	21.4−27.2	0.0029−0.045	0.0−0.14

dx.doi.org/10.1021/jp305933g | J. Phys. Chem. C 2012, 116, 18965−18972

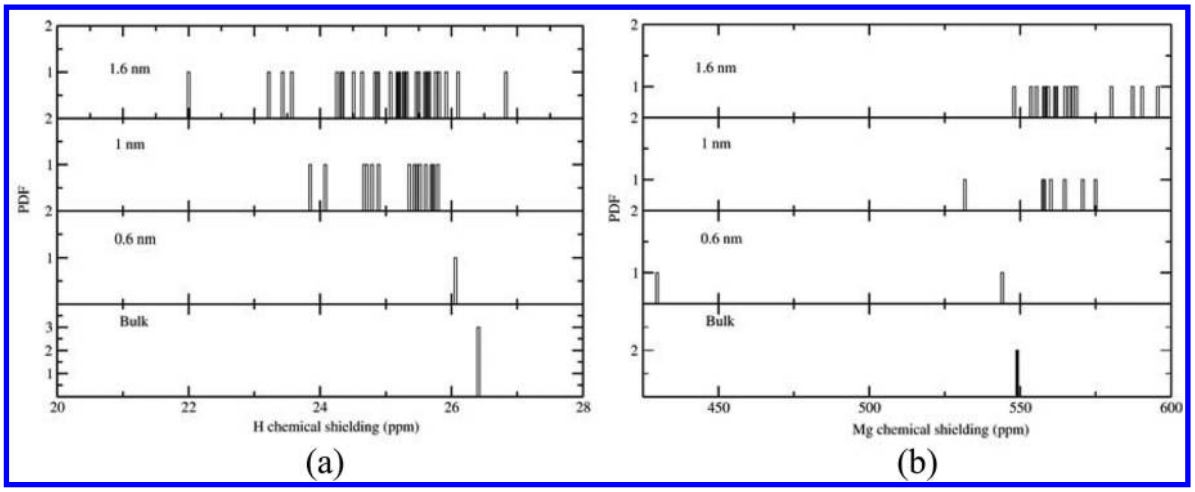

Figure 6. Calculated chemical shielding of H and Mg in different size of the nanowhiskers of MgH_2.

present study suggests that from the shift in the chemical shielding spectrum one can qualitatively classify the size of nanoparticles.

VII. CONCLUSION

In summary, theoretical study on the stability of nanoparticles and nanowhiskers of MgH_2 using ab initio total energy calculations was performed. From different polymorphs of MgH_2 we have constructed the nanoparticles and nanowhiskers. Among the studied nanoparticles, the β-MgH_2-derived nanoparticles are stable, while the α-MgH_2 derived nanowhiskers are more stable than those from other structural modifications. We have predicted that, depending on the nano-object (particles/whiskers), the internal structure will change. Similarly, the crystal structure plays a crucial role on the formation of nanostructures. Present theoretical prediction indicates that the critical size of the nanocluster and nanowhisker of different polymorphs-derived MgH_2 is below 2.4 and 1.83 nm, respectively. The NMR related parameters such as isotropic chemical shielding, quadrupolar coupling constant, and quadrupolar asymmetry parameter for different polymorphs of MgH_2 and selected nanophases properties were also calculated. The NMR study performed on nanoparticles and nanowhiskers of different sizes reveals that from the shift in the chemical shielding spectrum one can qualitatively classify the nanoparticle/whiskers size. The hydrogen site energy study suggests that it is easier to remove H from the stable nanocluster than that from the nanowhiskers and bulk phases. Several theoretical as well as experimental studies attempted to find the effect of pressure on the phase transitions for the polymorphs of MgH_2 but there is no general agreement on the obtained results. To make a firm conclusion about the high pressure behavior of MgH_2 more careful/accurate experimental and theoretical efforts are needed. The present study suggests that, in order to use MgH_2 as a hydrogen storage material, one must reduce the particle size below 2.4 nm. It may be a challenging task to prepare a bare nanoparticle of MgH_2 by mean of the existing experimental techniques. This can be overcome by encapsulation of such nanoparticles in nanoporous scaffold materials. From the experimental studies it was found that changes in thermodynamic stability will be small for confinement at $\geq$5 nm. But, the present study indicates that much smaller confinement ($\sim$1−2 nm) may be required for significant alteration. Further work is required to fully understand the effect of nanoconfinement on MgH_2.

AUTHOR INFORMATION

Corresponding Author

*E-mail: ponniahv@kjemi.uio.no.

Notes

The authors declare no competing financial interest.

ACKNOWLEDGMENTS

This work was funded by the European Union seventh framework program under the "NanoHy" (Grant Agreement No. 210092) project and Research Council of Norway funded Project 182040/S10 under the NANOMAT programme. P.V. gratefully acknowledges the Research Council of Norway for providing the computer time at the Norwegian supercomputer facilities and Karel Knížek for useful communications.

REFERENCES

(1) Buffat, Ph.; Borel, J.-P. *Phys. Rev. A* **1976**, *13*, 2287−2298.
(2) Shipway, A. N.; Katz, E; Willner, I. *Chem. Phys. Chem.* **2000**, *1*, 18−52.
(3) Lieber, C. M.; Wang, Z. L. *MRS Bull.* **2007**, *32*, 99−108.
(4) Link, S; El-Sayed, M. A. *Int. Rev. Phys. Chem.* **2000**, *19*, 409−453.
(5) Brower, F. M.; Matzek, N. E.; Reigler, P. F.; Rinn, H. W.; Roberts, C. B.; Schmidt, D. L.; Snover, J. A.; Terada, K. *J. Am. Chem. Soc.* **1976**, *98*, 2450−2453.
(6) Vajeeston, P.; Ravindran, P.; Hauback, B. C.; Fjellvåg, H.; Kjekshus, A.; Furuseth, S.; Hanfland, M. *Phys. Rev. B* **2006**, *73*, 224102.
(7) Zaluska, A.; Zaluski, L.; Ström-Olsen, J. O. *Appl. Phys. A: Mater. Sci. Process.* **2001**, *72*, 157−165.
(8) Orimo, S.; Fujii, H.; Ikeda, K. *Acta Mater.* **1997**, *45*, 331−341.
(9) Zaluska, A.; Zaluski, L.; Ström-Olsen, J. O. *J. Alloys Compd.* **1999**, *288*, 217−225.
(10) Hanada, N.; Ichikawa, T.; Fujii, H. *J. Phys. Chem. B* **2005**, *109*, 7188−7194.
(11) Lu, J.; Choi, Y. J.; Fang, Z. Z.; Sohn, H. Y.; Ronnebro, E. *J. Am. Chem. Soc.* **2009**, *131*, 15843−15852.
(12) Zhang, Y.; Tian, Q.; Chu, H.; Zhang, J.; Sun, L.; Sun, J.; Wen, Z. *J. Phys. Chem. C* **2009**, *113*, 21964−21969.
(13) Jin, S. A.; Shim, J. H.; Cho, Y. W.; Yi, K. W. *J. Power Sources* **2007**, *172*, 859−62.
(14) Xie, L.; Liu, Y.; Wang, Y. T.; Zheng, J. *Acta Mater.* **2007**, *55*, 4585−91.
(15) Lu, J.; Choi, Y. J.; Fang, Z. Z.; Sohn, H. Y.; Ronnebro, E. *J. Am. Chem. Soc.* **2010**, *132*, 6616−6623.

(16) Mao, J.; Guo, Z.; Leng, H.; Wu, Z.; Guo, Y.; Yu, X.; Liu, H. *J. Phys. Chem. C* **2010**, *114*, 11643−11649.
(17) Huot, J.; Pelletier, J. F.; Lurio, L. B.; Sutton, M.; Schulz, R. *J. Alloys Compd.* **2003**, *348*, 319−324.
(18) Lillo-Ródenas, M. A.; Aguey-Zinsou, K. F.; Cazorla-Amorós, D.; Linares-Solano, A.; Guo, Z. X. *J. Phys. Chem. C* **2008**, *112*, 5984−5992.
(19) Mao, J. F.; Wu, Z.; Chen, T. J.; Weng, B. C.; Xu, N. X.; Huang, T. S.; Guo, Z. P.; Liu, H. K.; Grant, D. M.; Walker, G. S.; Yu, X. B. *J. Phys. Chem. C* **2007**, *111*, 12495−12498.
(20) Oelerich, W.; Klassen, T.; Bormann, R. *J. Alloys Compd.* **2001**, *315*, 237−242.
(21) Huot, J.; Liang, G.; Schultz, R. *Appl. Phys. A: Mater. Sci. Process.* **2001**, *72*, 187−195.
(22) Blöchl, P. E. *Phys. Rev. B* **1994**, *50*, 17953−17979. Kresse, G.; Joubert, D. *Phys. Rev. B* **1999**, *59*, 1758−1775.
(23) Kresse, G.; Hafner, J. *Phys. Rev. B* **1993**, *47*, 558−561. Kresse, G.; Furthmuller, J. *Comput. Mater. Sci.* **1996**, *6*, 15−50.
(24) Perdew, J. P.; Burke, K.; Ernzerhof, M. *Phys. Rev. Lett.* **1996**, *77*, 3865−3868.
(25) Perdew, J. P.; Chevary, J. A.; Vosko, S. H.; Jackson, K. A.; Pederson, M. R.; Singh, D. J.; Fiolhais, C. *Phys. Rev. B* **1992**, *46*, 6671−6687.
(26) Clark, S. J.; Segall, M. D.; Pickard, C. J.; Hasnip, P. J.; Probert, M. J.; Refson, K.; Payne, M. C. *Z. Kristallogr.* **2005**, *220*, 567−570.
(27) Perdew, J. P. *Electronic Structure of Solids*; Ziesche, P., Eschrig, H., Eds.; Akademie: Berlin, 1991; p 11; Perdew, J. P.; Burke, K.; Wang, Y. *Phys. Rev. B* **1996**, *54*, 16533−16539. Perdew, J. P.; Burke, K.; Ernzerhof, M. *Phys. Rev. Lett.* **1996**, *77*, 3865−3868.
(28) Bastide, J. P.; Bonnetot, B.; Letoffe, J. M.; Claudy, P. *Mater. Res. Bull.* **1980**, *15*, 1215−1219.
(29) Zachariasen, W. H.; Holley, C. E., Jr; Stamper, J. F., Jr *Acta Crystallogr., Sect. A* **1963**, *16*, 352−353.
(30) Bortz, M.; Bertheville, B.; Böttger, G.; Yvon, K. *J. Alloys Compd.* **1999**, *287*, L4−L6.
(31) Vajeeston, P.; Ravindran, P.; Kjekshus, A.; Fjellvåg, H. *Phys. Rev. Lett.* **2002**, *89*, 175506.
(32) Cui, S.; Feng, W.; Hu, H.; Feng, Z.; Wang, Y. *Solid State Commun.* **2008**, *148*, 403−405.
(33) Moriwaki, T.; Akahama, Y.; Kawamura, H. *J. Phys. Soc. Jpn.* **2006**, *75*, 074603.
(34) Song, Y.; Guo, Z. X. *Appl. Phys. Lett.* **2006**, *89*, 111911.
(35) Zhang, L. J.; Wang, Y. C.; Cui, T.; Li, Y.; Li, Y. W.; He, Z.; Ma, Y. M.; Zou, G. T. *Phys. Rev. B* **2007**, *75*, 144109.
(36) Kohlmann, H.; Zhao, Y.; Nicol, M. F.; McClure, J. *Z. Kristallogr.* **2008**, *223*, 706−710.
(37) Moser, D.; Bull, D. J.; Cowpe, J. S.; Roach, D. L.; Ross, D. K.; Noréus, D.; Tucker, M. G. *High Pressure Res.* **2010**, *30*, 643−652.
(38) Srinivasan, R.; Rice, L.; Davis, B. H. *J. Am. Ceram. Soc.* **1990**, *73*, 3528−3530.
(39) Wagemans, R. W. P.; van Lenthe, J. H.; de Jough, P. E.; van Dillen, A. J.; de Jong, K. P. *J. Am. Chem. Soc.* **2005**, *127*, 16675−16680.
(40) Cheung, S.; Deng, W. Q.; van Duin, A. C. T.; Goddard, W. A. *J. Phys. Chem. A* **2005**, *109*, 851−859.
(41) Kim, K. C.; Dai, B.; Johnson, J. K.; Sholl, D. S. *Nanotechnology* **2009**, *20*, 204001.
(42) Kyoi, D.; Sato, T.; Rönnebro, E.; Kitamura, N.; Ueda, A.; Ito, M.; Katsuyama, S.; Hara, S.; Noréus, D.; Sakai, T. *J. Alloys Compd.* **2004**, *372*, 213−217.
(43) Gross, A. F.; Ahn, C. C.; Van Atta, S. L.; Liu, P.; Vajo, J. J. *Nanotechnology* **2009**, *20*, 204005.
(44) Zhang, S.; Gross, A. F.; Van Atta, S. L.; Lopez, M.; Liu, P.; Ahn, C. C.; Vajo, J. J.; Jensen, C. M. *Nanotechnology* **2009**, *20*, 204027.
(45) Cuevas, F.; Korablov, D.; Latroche, M. *Phys. Chem. Chem. Phys.* **2012**, *14*, 1200−1211.
(46) Paskevicius, M.; Sheppard, D. A.; Buckley, C. E. *J. Am. Chem. Soc.* **2010**, *132*, 5077−5083.
(47) Zhao-Karger, Z.; Hu, J.; Roth, A.; Wang, D.; Kübel, C.; Lohstroh, W.; Fichtner, M. *Chem. Commun.* **2010**, *46*, 8353−8355.
(48) Zlotea, C.; Lu, J.; Andersson, Y. *J. Alloys Compd.* **2006**, *426*, 357−362.
(49) Saita, I.; Toshima, T.; Tanda, S.; Akiyama, T. *Mater. Trans.* **2006**, *47*, 931−934.